Phase diagram of $LaVO_3$ under epitaxial strain: Implications for thin films grown on $SrTiO_3$ and $LaAlO_3$ substrates

Hongming Weng* and Kiyoyuki Terakura

Research Center for Integrated Science, Japan Advanced Institute of Science and Technology, Nomi, Ishikawa 923-1292, Japan and CREST, JST, 4-1-8 Honcho, Kawaguchi, Saitama 332-0012, Japan

(Received 31 May 2010; revised manuscript received 9 August 2010; published 7 September 2010)

Various exotic phenomena have been observed in epitaxially grown films and superlattices of transition-metal oxides. In these systems, not only the interface properties but also the strain-induced modification in the bulk properties play important roles. With the recent experimental activities [Y. Hotta, T. Susaki, and H. Y. Hwang, Phys. Rev. Lett. **99**, 236805 (2007)] in mind, we have studied the epitaxial strain effects on the electronic structure of Mott insulator $LaVO_3$. The present work is based on the calculations using density-functional theory supplemented by adding local Coulomb repulsion U for V d orbitals. The range of strain studied here extends from $c/a=0.98$ (bulk $LaVO_3$ case) to $c/a=1.107$ ($LaAlO_3$ substrate case). In this range of the strain, we have found the following three different antiferromagnetic spin-ordering (SO) phases. For $0.98<c/a<1.005$, the combination of C-type SO and G-type orbital ordering (OO) is the most stable. The bulk $LaVO_3$ belongs to this range. For $1.005<c/a<1.095$, the ground state has A-type SO and G-type OO. $LaVO_3$ epitaxially grown on $SrTiO_3$ is in this range. When $c/a>1.095$, G-type SO with ferromagnetic OO becomes the ground state. This range includes the case of $LaAlO_3$ substrate. The implications of these results with regard to the experimental data for thin films of $LaVO_3$ on $SrTiO_3$ and $LaAlO_3$ substrates will be described. Detailed discussion is given on the mechanisms of stabilizing particular combination of SO and OO in each of three phases.

DOI: 10.1103/PhysRevB.82.115105 PACS number(s): 71.27.+a, 75.25.−j, 75.10.Dg

I. INTRODUCTION

The interface of two different transition-metal oxides has attracted intensive studies since various unusual electronic states have been observed in that region. The metallic n-type interface between two band insulators $LaAlO_3$ and $SrTiO_3$,[1–5] as well as that between Mott insulator $LaVO_3$ and band insulator $SrTiO_3$ (Ref. 6) has stimulated broad interests. Both of the systems have the so-called "polar discontinuity" problem once the perovskite $LaAlO_3$ or $LaVO_3$ grows on the $SrTiO_3$ substrate along [001] direction. The variation of valence state of transition-metal ions brings a new degree of freedom to resolve the polar discontinuity problem by accepting proper number of electrons in the n-type interface region. In addition to the electronic reconstruction, oxygen vacancy introduced during growth[7] is also proposed to be one of the origin of conducting interface. On the contrary, the p-type interfaces of the above two are insulating even if holes are believed to be introduced due to the same electronic reconstruction mechanism. In $LaAlO_3/SrTiO_3$ case, it is proposed that the induced holes are compensated by electrons generated by oxygen vacancy. In fact, existence of appreciable amount of O^{2-} vacancies was detected.[2] In $LaVO_3/SrTiO_3$ case, the possibility of existing oxygen vacancy is not fully excluded since annealing in oxygen will lead to $LaVO_4$ instead of $LaVO_3$. Nevertheless, two dimensional metallic conductivity was clearly observed for the n-type interface while the p-type interface was insulating.[6] Jackeli and Khaliullin[8] addresses the mechanism of insulating behavior for the p-type interface. Considering the active t_{2g} electrons are strongly correlated and confined in the two-dimensional VO_2 layer, they proposed a combined orbital, charge, and magnetic ordering in the VO_2 interface layer when it is half doped with holes. The resulted insulating state is consistent with the experimental observation but the proposed magnetic character has not yet been experimentally verified. In $LaVO_3/SrVO_3$ superlattice structure with a similar p-type interface, conducting and room-temperature ferromagnetic (FM) VO_2 layer is observed.[9]

In addition to the carrier doping, the epitaxially grown films may have another important effect, the epitaxial strain effect. While, for the epitaxial film of $LaAlO_3$, the strain may produce only moderate effects on the electronic structure by distorting the band structure to some extent, for that of $LaVO_3$, as well as many other transition-metal oxides with partially occupied d bands, the epitaxial strain may induce phase transitions and may serve as a way to tune physical properties. For example, the strain effect is used to tune magnetic properties of $SrRuO_3$ (Ref. 10) and to control the transport properties through magnetic phase transition in $La_{1-x}Sr_xMnO_3$ (Ref. 11) and $Ca_{1-x}Ce_xMnO_3$.[12,13] These are the manifestation of the well-known strong coupling among lattice, spin, orbital, and charge degrees of freedom of correlated d electrons. We demonstrate in the following that the strain effects on the magnetic and orbital orderings are crucially important also for $LaVO_3$ epitaxially grown on $SrTiO_3$ and $LaAlO_3$. We emphasize that the physics controlling the strain effects in $LaVO_3$ is quite different from those in $SrRuO_3$ and manganites. In $SrRuO_3$, Ru is in 4+ state with d^4 configuration. Because of relatively extended character of $4d$ orbitals, $SrRuO_3$ is in the low spin state and the Fermi level lies in the minority-spin t_{2g} band. However, there is no phase transitions among different ordered magnetic states due to weak Coulomb interaction. In contrast of $SrRuO_3$, Mn $3d$ orbitals have stronger localization and both of $La_{1-x}Sr_xMnO_3$ and $Ca_{1-x}Ce_xMnO_3$ take high spin state with the Fermi level

in the majority-spin e_g band. However, despite its localized nature of Mn $3d$ orbitals, e_g orbitals can strongly hybridize with the oxygen p orbitals to form e_g band with appreciable bandwidth and the electron correlation effect becomes weaker. The strain effect on e_g bands can be understood in a straight manner in terms of lattice effects on the p-d hybridization. On the other hand, t_{2g} band of $LaVO_3$ is quite narrow due to weak p-d hybridization. Because of this, the competition between the lattice distortion and strong correlation effect produces the complexity in the physics of strain effects. As far as we know, no theoretical work is available to date which addresses the strain effects in t_{2g} systems of $3d$ transition-metal oxides.

Even in bulk $LaVO_3$, understanding of coexistence of C-type spin ordering (C-SO) and G-type orbital ordering (G-OO) is still a matter of controversy. There have been many arguments on which of Jahn-Teller (JT) distortion[14,15] or orbital fluctuations[16–18] is dominant. The V^{3+} ion surrounded by an oxygen octahedron has two electrons on the t_{2g} orbitals, which are threefold degenerate in the cubic symmetry. Energy gain can be achieved by lifting this orbital degeneracy through cooperative JT distortion of VO_6 octahedra and put the electrons into the lower-energy orbitals. The fluctuation of orbital degrees of freedom thus is suppressed by forming corresponding orbital ordering regardless of spin ordering. On the other hand, it is generally expected that the JT distortion in the t_{2g} system is rather small[18] and that Coulomb interaction between localized t_{2g} electrons leads to quite strong correlations among the orbital, spin, and charge degrees of freedom. This is the background of theoretical works treating the orbital degrees of freedom and the spin degrees of freedom on the equal footing using Kugel-Khomskii superexchange (SE) interaction models.[16,19,20] Such SE interaction is strongly frustrated on a perovskite lattice, leading to enhanced quantum effect like orbital fluctuations. Khaliullin *et al.*[16] proposed that orbital fluctuations stabilize G-OO and C-SO in cubic vanadates. On the other hand, Fang *et al.*[15] have argued that the JT distortion suppresses the quantum orbital fluctuations in $LaVO_3$, as well as in YVO_3. The SO and OO in both vanadates can be well understood in terms of JT distortion within their density-functional theory (DFT) calculations. In addition, the splitting of spin-wave dispersions in YVO_3 with C-SO is attributed to the reduced geometrical symmetry instead of orbital-Peierls state.[17] Their prediction of the similar splitting of spin-wave dispersion in $LaVO_3$ is observed experimentally by Tung *et al.*[21] While again orbital fluctuations have been shown to be quite strong in $LaVO_3$ and can be suppressed only in the monoclinic phase by both JT and $GdFeO_3$-type distortion by using DFT+dynamical mean-field theory calculations.[22] Recently, Kugel-Khomskii SE model improved by including $GdFeO_3$-type distortion[18] is used to explain the observed phase diagram of a serials of RVO_3 (R is rare earth element or Y) perovskites. It is found that the lattice strain effect can partially suppress the orbital fluctuations, although JT distortion is not considered there. In reality, the situation is more complicated by the coexisting of both JT and $GdFeO_3$-type distortions.

In this work, we will tune the strength of lattice distortion directly by applying external tetragonal strain and study how lattice distortion and SE work together to lead to evolution of different SO and OO in $LaVO_3$ as c/a is varied. This analysis will sever as the starting point to understand the interface of the thin film of $LaVO_3$ grown on $SrTiO_3$ and $LaAlO_3$. We predict that the stable SO for the tetragonal strain corresponding to $SrTiO_3$ ($LaAlO_3$) substrate will be A type (G type) keeping the insulating state unchanged. The result is at least qualitatively consistent with the experimental observation that the interface with the $SrTiO_3$ substrate can be metallic[6] while that with $LaAlO_3$ is insulating[23] because the FM intraplane SO within the interface VO_2 layer will become metallic more easily than the antiferromagnetic (AF) intraplane SO when holes or electrons are doped. Moreover, the observation of anomalous Hall effect for the interface with $SrTiO_3$ implies that the FM SO must exist at the interface. This is compatible with A-SO but incompatible with C-SO and G-SO. Nevertheless, more elaborate calculations are needed to clarify the effects of interface and they are left as our next step task.

We also try to clarify the crystal-field effect coming from $GdFeO_3$-type distortion and point out that the detailed geometrical structure is important to determine the SO and OO in $LaVO_3$. In the next section, we will describe the setting up of the problem, computational details of the DFT+U calculation and the basic theoretical framework for the analysis of stability of SO and OO. The results and discussion will be given in Sec. III. Finally, we make a summary in Sec. IV.

II. METHODOLOGY

Experimentally, $LaVO_3$ grown on $SrTiO_3$ (Ref. 6) and $LaAlO_3$ (Ref. 23) is found to be fully constrained to the substrate and the lattice volume is found to be close to its bulk in $LaAlO_3$ case.[23] Thus, the a and b lattice constants of $LaVO_3$ are taken as those of the substrate and c lattice constant is taken by keeping the unit-cell volume the same as the experimental monoclinic $LaVO_3$.[24] The strained tetragonal $LaVO_3$ with c/a ranging from 0.98 to 1.11 are studied. The calculations are done with QMAS (Ref. 26) code based on the projector augmented-wave (PAW) method. The pseudopotentials are generated with the valence configurations of $5s^25p^65d^06s^26p^1$ for La, $3s^23p^63d^34s^24p^0$ for V, and $2s^22p^4$ for O. The expression for the exchange-correlation energy is the one parametrized by Perdew *et al.*[27] within generalized gradient approximation (GGA). The cut-off energy for the plane-wave basis is taken as 35 Ry. A grid of $6\times6\times5$ is used to sample the full Brillouin zone during the self-consistent calculation. To take account of the strong on-site Coulomb interaction of V $3d$ electrons, rotationally invariant +U method[28] is used with effective U_{eff} parameter being 3.0 eV, which can properly reproduce the band gap of bulk $LaVO_3$.[15] In order to study AF ordering, a pseudocubic supercell of $\sqrt{2}\times\sqrt{2}\times2$ is used, which includes four V ions with V1 and V2 in one ab layer while V3 and V4 on top of V1 and V2, respectively. The global axes x, y, and z at V sites are defined as the [110], [$\bar{1}$10], and [001] directions of the unit cell (see Fig. 6), respectively. With these settings, calculations are performed for the free bulk $LaVO_3$ at 10 K and it is found that the energy differences among four stud-

ied SOs, including FM, *A*-type (AF stacking of FM *ab* layers), *C*-type (FM stacking of AF *ab* layers), and *G*-type (AF staking of AF *ab* layers) AF spin orderings, are comparable with those in Ref. 15. For $LaVO_3$ under different epitaxial strain, the atomic position is fully relaxed within each SO until the forces are less than 0.01 eV/Å.

To analyze the underlying mechanism of obtained results, maximally localized Wannier functions (MLWFs) (Ref. 29) for t_{2g} bands are constructed by using OPENMX code.[30,31] We have constructed MLWFs for V t_{2g} bands in two ways. One is done for the nonmagnetic state of $LaVO_3$ within GGA calculations. The crystal structure is assumed to be the one optimized in the GGA+U calculation for the most stable SO for a given c/a. In this approach, the crystal field and the covalent effect are self-consistently taken into account. Since t_{2g} bands form isolated group of bands, disentangling procedure is not necessary. The crystal-field orbitals (CFOs), orbital energies, and hopping integrals can be obtained through the Hamiltonian within the space of MLWFs. The Hubbard model is then constructed by adding the U term. The SE interaction among these CFOs is calculated within the Hubbard model where hopping between nearest-neighboring (NN) sites is treated as perturbation.[16,32] Considering V^{3+} ion is in the high spin state, the initial configuration is such that the two of the three CFOs are occupied with parallel spin moment. The neighboring sites can be ferromagnetically or antiferromagnetically ordered. Taking into account all the possible virtual hopping paths, the energy gains for FM and AF configurations within the second-order perturbation treatment are

$$\Delta E_{\mathrm{FM}} = \sum_{j,j'} \sum_{i=1,2} -\frac{|t_{i,3}^{j,j'}|^2}{U} \frac{1}{1-3\frac{J_{\mathrm{H}}}{U}} \tag{1}$$

and

$$\Delta E_{\mathrm{AF}} = \sum_{j,j'} \left\{ \sum_{i,i'=1,2} -\frac{|t_{i,i'}^{j,j'}|^2}{U} \frac{1+\frac{J_{\mathrm{H}}}{U}}{1+2\frac{J_{\mathrm{H}}}{U}} + \sum_{i=1,2} -\frac{|t_{i,3}^{j,j'}|^2}{U} \frac{1-2\frac{J_{\mathrm{H}}}{U}}{1-3\frac{J_{\mathrm{H}}}{U}} \right\}, \tag{2}$$

respectively. Here $t_{i,i'}^{j,j'}$ means the hopping integral from orbital i on site j to orbital i' on site j'. Among the three CFOs, the first ($i=1$) one and the second one ($i=2$) are fully occupied while the third one ($i=3$) is empty. We have neglected the crystal-field splittings among these three CFOs in the above derivation since they make only small contributions to the SE interaction, though it is straightforward to include them. In fact in order to compare total energies among different OO in the following section, we take account of the difference in the on-site energy of occupied orbitals. J_{H} and U are the Hund coupling and intraorbital Coulomb interaction of V^{3+} ion.

The approach described above can be straightforwardly applied to the analysis in region (a) and region (c) in Fig. 1, where OO and JT distortion are not sensitive to SO. On the other hand, as will be shown later, the situation in the intermediate case in region (b) is rather subtle in the sense that OO and JT distortion depend on SO more sensitively. In order to treat such a case, we adopt an alternative approach in which the MLWFs are constructed for each SO within GGA+U calculations.[33] As the t_{2g} bands are entangled with V e_g bands in this case, the minimum outer window is set to cover all the t_{2g} bands. At the same time the maximum inner window including all the bands purely from t_{2g} orbitals is used. The crystal-field effect, covalent effect, and U effect are now considered on equal footing self-consistently and these MLWFs are used to evaluate the magnetic interaction energy in each SO by using the SE mechanism. This treatment will be found to be more precise than the first one if the crystal field and SE interaction from spin-orbital coupling are comparable with each other.

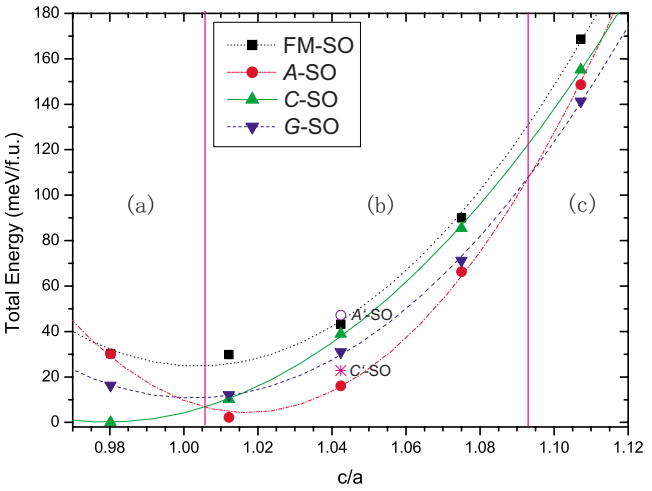

FIG. 1. (Color online) The total energies of $LaVO_3$ with FM-, *A*-, *C*-, and *G*-AF SO under different epitaxial strain (measured by c/a value). A'-SO and C'-SO denote *A*-type and *C*-type SOs, respectively, with the principal axis lying in the x direction (Fig. 6). The zero-energy point has been shifted to the total energy of *C*-SO in $LaVO_3$ with $c/a=0.98$. Note that the results are obtained with an assumption that the volume of $LaVO_3$ is conserved. See comments in Ref. 24.

In both approaches, the obtained MLWFs with spreads converging to 10^{-10} Å^2 are mostly centered around each V atoms and very similar to the atomic t_{2g} orbitals. The interpolated band structure well reproduces the original band structure.

III. RESULTS AND DISCUSSIONS

The total energies with different long-range SO, including FM, *A*-, *C*-, and *G*-type AF orderings, for $LaVO_3$ under different epitaxial strain (measured by c/a value) are plotted in Fig. 1. Three regions can be easily identified. For (a) $c/a < 1.005$, *C*-SO is the most stable one, which is consistent with the SE model result for ideal cubic structure with $c/a=1.0$ (Ref. 16) and other DFT-based calculations for experimental monoclinic $LaVO_3$ with c/a nearly 0.98.[15,34,35] Here, the tetragonal $LaVO_3$ with $c/a=0.98$ is denoted as t-LVO.

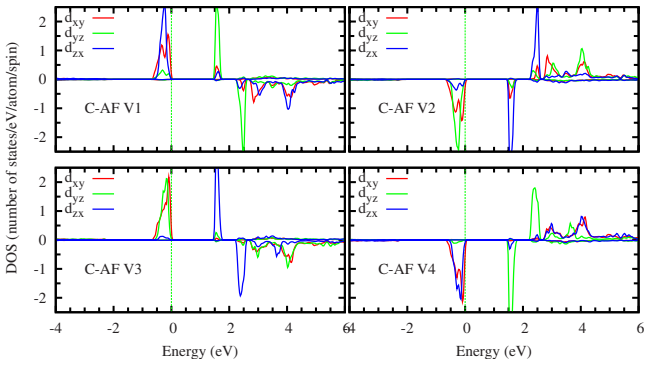

FIG. 2. (Color online) The partial density of states of t_{2g} orbitals for V ions in $LaVO_3$ with $c/a=0.98$ with C-SO and G-OO. Fermi level is set at 0.0 eV.

For (b) $1.005<c/a<1.095$, A-SO becomes the stablest one. $LaVO_3$ grown on $SrTiO_3$ (denoted as LVO/STO) is located in this region with $c/a=1.01$. For (c) $c/a>1.095$, G-SO becomes the one with the lowest total energy and $LaVO_3$ grown on $LaAlO_3$ (denoted as LVO/LAO) is in this region with $c/a=1.107$. In addition to A-SO and C-SO with the principal axis along the c axis, we studied other possible A-SO and C-SO with the principal axis along the x axis (Fig. 6) (called A'-SO and C'-SO here) only for the case of c/a close to 1.04. Although the total energy of C'-SO is rather close to that of A-SO as can be seen in Fig. 1, these SOs are not the lowest energy ordering. In this paper, we do not discuss these SOs any further. In the following we discuss mechanisms stabilizing particular SO and OO in each region of Fig. 1 only in the case of the principal axis lying along the c direction.

A. Region (a)

The self-consistent GGA+U calculation was performed for $c/a=0.98$ (t-LVO) with structure optimization for all the four SOs. The calculated partial density of states (p-DOS) for the most stable combination of SO and OO is shown in Fig. 2. One electron occupies the d_{xy} orbital on all V sites and the other one occupies the d_{zx}, d_{yz}, d_{yz}, and d_{zx} orbitals at V1, V2, V3, and V4, respectively. This G-OO is found for all the four types of SO like in other calculations[15,16,34,35] and consistent with the JT distortion pattern. The p-DOS is qualitatively the same for other SO. An important observation is that in contrast to the result of GGA calculation[14] the present p-DOS is well characterized by the Hubbard model with the rotationally invariant form of the local Coulomb interaction as shown in Fig. 3, which is a schematic view of the p-DOS at V1 and V4 sites. For V2 and V3 sites, the d_{yz} and d_{zx} orbitals are exchanged in Fig. 3. We can now discuss the intersite magnetic coupling using the information in p-DOS in Figs. 2 and 3. Within the G-OO, if local moments on V1 and V2 [in the x (y) direction] are arranged ferromagnetically as shown in Fig. 4(a), the energy gain comes from the $dd\pi$-type hopping of electrons on d_{zx} (d_{yz}) orbitals. If they are arranged in AF configuration [Fig. 4(b)], another $dd\pi$-type hopping of electrons on d_{xy} orbitals contributes to energy gain in addition to the hopping of d_{zx} (d_{yz}) electrons. This additional

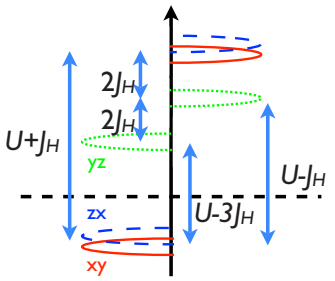

FIG. 3. (Color online) Schematic energy diagram of d^2 t_{2g} orbitals from the Hubbard model with the rotationally invariant form of the local Coulomb interaction. This diagram corresponds to the p-DOS at V1 and V4 sites in Fig. 2. Here U is the intraorbital Coulomb interaction and J_H is Hund's coupling. The vertical single arrow indicates the increasing of energy. Its left side is for the spin-up channel and the right side is for the spin down. The horizontal dashed line marks the Fermi level. The energy level separations are shown by vertical double arrows.

energy gain makes the AF ordering more stable in the ab layer in the reasonable range of J_H. Along the c direction [Figs. 4(c) and 4(d)], FM configuration has more kinetic-energy gain from the $dd\pi$-type hopping of d_{yz}/d_{zx} electrons than the AF one due to finite J_H. Note that the hopping between d_{xy} orbitals in the c direction is of $dd\delta$ type and makes only two orders of magnitude smaller contribution to the magnetic interaction energy than the contribution from the hopping of $dd\pi$ type. The basic idea of the FM superexchange along the c direction is that the alternating occupation of d_{yz} and d_{zx} orbitals at V sites along the c direction produces the situation of superexchange between orthogonal orbitals. The above arguments imply that the SE interaction evolves the C-SO with G-OO near the cubic lattice case[16] if temperature is low enough. The G-type orbital polarization induces G-type JT distortion to gain more electronic energy.

The stability of C-SO and G-OO in region (a) is further supported by an analysis based on Eqs. (1) and (2) (Ref. 36) using a simple model cubic system as described in Appendix A. In this analysis, the above combination of G-OO and

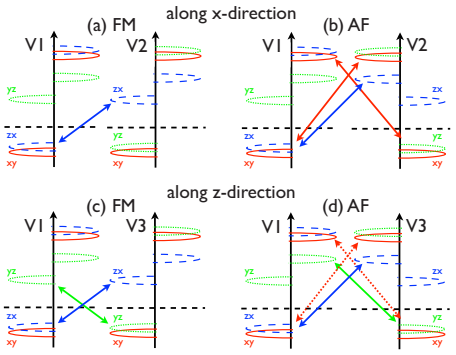

FIG. 4. (Color online) Schematic pictures of magnetic coupling between V1 and V2 ions along x direction ordered in (a) FM and (b) AF configurations. Those between V1 and V3 along z direction ordered in (c) FM and (d) AF configurations are also shown. The virtual hopping paths bringing energy gain in each case are indicated by solid arrows. The dashed arrows in (d) are the paths which can make only negligible contribution to the magnetic coupling.

TABLE I. The linear combination coefficients in the t_{2g} orbital basis of crystal-field orbitals on V ions in MLWF basis for t-LVO (c/a=0.98), LVO/STO (c/a=1.01), and LVO/LAO (c/a=1.11). The bold numbers indicate the largest component among three t_{2g}-like MLWFs. The on-site energy increases from CF1 to CF3. In each case, the optimized structure with SO in the ground state is used.

t-LVO (c/a=0.98)		d_{xy}	d_{zx}	d_{yz}		d_{xy}	d_{zx}	d_{yz}
V1	CF1	**−0.838**	−0.507	−0.203	V2	**0.838**	0.204	−0.507
	CF2	−0.352	0.218	**0.910**		−0.353	**0.910**	−0.217
	CF3	−0.417	**0.834**	−0.361		−0.417	−0.361	**−0.834**
V3	CF1	−0.849	0.512	−0.129	V4	**−0.849**	−0.129	−0.512
	CF2	0.471	**0.626**	−0.621		−0.472	0.621	**0.626**
	CF3	0.237	0.588	**0.773**		0.238	**0.773**	−0.588
LVO/STO (c/a=1.01)		d_{xy}	d_{zx}	d_{yz}		d_{xy}	d_{zx}	d_{yz}
V1	CF1	0.159	−0.020	**0.987**	V2	−0.149	**0.988**	−0.024
	CF2	0.158	**−0.986**	−0.046		0.154	0.046	**0.987**
	CF3	**0.975**	0.163	−0.154		**0.977**	0.145	−0.159
V3	CF1	−0.161	−0.019	**0.987**	V4	−0.174	**−0.984**	0.026
	CF2	0.163	**0.986**	0.050		−0.165	0.055	**0.985**
	CF3	**−0.973**	0.169	−0.155		**−0.971**	0.167	−0.172
LVO/LAO (c/a=1.11)		d_{xy}	d_{zx}	d_{yz}		d_{xy}	d_{zx}	d_{yz}
V1	CF1	−0.145	−0.227	**0.963**	V2	0.145	**0.963**	−0.227
	CF2	0.023	**−0.974**	−0.227		0.023	0.226	**0.974**
	CF3	**0.989**	−0.010	0.146		**−0.989**	0.146	−0.011
V3	CF1	0.144	−0.229	**0.963**	V4	−0.144	**0.963**	−0.228
	CF2	0.023	**0.973**	0.228		−0.023	0.227	**0.974**
	CF3	**−0.989**	−0.010	0.145		**−0.989**	−0.145	0.010

C-SO is the most stable one for $0<J_H/U<0.24$, which is consistent with the result of Ref. 16. In the actual $LaVO_3$, a reasonable value of J_H/U is around 0.2.[15,16,22,34,35]

We now proceed to the step of estimating quantitatively the magnetic coupling between neighboring magnetic moments using Eqs. (1) and (2). In the actual systems, not only JT distortion but also rotation and tilt of oxygen octahedron are present. These lattice distortions will lead to splittings and/or mixing among three t_{2g} orbitals to form new basis set, CFOs, which are more suitable basis set for the SE analysis.[32] The CFOs and their splittings are obtained by diagonalizing the on-site real-space Hamiltonian in the subspace of MLWFs constructed from t_{2g} bands within nonspin-polarized GGA calculations.[32,34] The linear combination coefficients of CFO in the t_{2g} orbital basis is shown in Table I. As shown in Fig. 5, for t-LVO the splitting between the high and middle CFOs is 62 meV for V1 and V2 (48 meV for V3 and V4, not shown). This splitting is much smaller than the energy level splitting in Figs. 2 and 3 which is governed mainly by Coulomb parameters. Nevertheless, the fact that the crystal-field splitting pattern among different V sites is consistent with the energy diagram in Fig. 3 implies that the crystal-field splitting may be the trigger for producing the orbital ordering which is strongly stabilized by the Coulomb interaction. The neighboring hopping integrals between CFOs can be estimated by using MLWF and are listed in Table II.[37] Substituting those for t-LVO into Eqs. (1) and (2), the magnetic coupling J_{ij} between neighboring Vi and Vj sites can be obtained within the assumption that the lowest two CFOs are both singly occupied.[16,22] For t-LVO with J_H/U=0.2 and U=3.0 eV, J_{12} (J_{34}) is 6.8 (3.1) meV and $J_{13}=J_{24}=-10.2$ meV, being consistent with the *C*-SO in the

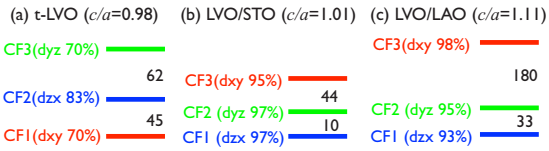

	t-LVO	LVO/STO	LVO/LAO
$4t_{ab}^2/U$	30	32	34
$4t_c^2/U$	36	32	20

FIG. 5. (Color online) The CFOs and their splittings in (a) t-LVO (b) LVO/STO, and (c) LVO/LAO listed in Table I. The main component of each CFOs is indicated in the parentheses. Here only V1 site is shown for each case. In each of three cases (a), (b), and (c), the position of CFO mostly composed of d_{xy} orbital is the same for all V sites [the lowest for (a) and the highest for (b) and (c)], while those of d_{zx} and d_{yz} are altered from site to site as shown in Table I. t_{ab} is the averaged hopping integrals between CFOs in the *ab* layer and t_c is that in the *c* direction from Table II. U is taken as 3.0 eV and all other energies are in millielectron volt.

TABLE II. The hopping integrals (in meV) between crystal-field orbitals for t-LVO (c/a=0.98), LVO/STO (c/a=1.01), and LVO/LAO (c/a=1.11) listed in Table I.

t-LVO (c/a=0.98)		CF1	CF2	CF3		CF1	CF2	CF3
V1-V2	CF1	−161.59	67.39	38.89	V1-V3	2.67	38.01	99.32
	CF2	62.25	−40.11	138.17		−40.93	40.19	−162.62
	CF3	−9.63	26.91	24.19		−82.78	−161.62	−65.81
V3-V4	CF1	124.35	85.81	−31.06	V2-V4	−2.79	38.02	−99.42
	CF2	−68.23	−4.19	35.09		−41.20	−39.90	−161.88
	CF3	118.03	−110.66	13.93		−82.80	161.88	−65.93
LVO/STO (c/a=1.01)		CF1	CF2	CF3		CF1	CF2	CF3
V1-V2	CF1	80.60	−0.69	−83.00	V1-V3	−164.86	11.47	64.23
	CF2	134.95	72.37	−76.30		−9.08	141.63	17.57
	CF3	−47.25	−49.25	−141.46		62.27	−17.36	11.00
V3-V4	CF1	−81.69	140.22	44.71	V2-V4	165.24	−10.04	61.18
	CF2	−2.61	−70.77	−49.23		9.33	−140.93	15.94
	CF3	−80.14	75.21	−139.12		−65.96	17.97	10.93
LVO/LAO (c/a=1.11)		CF1	CF2	CF3		CF1	CF2	CF3
V1-V2	CF1	90.56	−20.78	−62.34	V1-V3	−135.30	3.61	5.19
	CF2	163.77	−102.73	−95.30		−3.96	107.38	1.98
	CF3	−40.68	−2.78	−157.14		5.05	−2.01	29.65
V3-V4	CF1	91.03	−163.93	−40.49	V2-V4	−135.43	−3.53	5.17
	CF2	−21.16	102.97	−2.80		−4.00	−107.35	2.00
	CF3	62.65	−95.27	157.12		−5.05	−1.95	−29.66

ground state. The nonequivalent J and CF splittings in two ab layers indicate the different lattice distortion in two layers.[15]

We give here a brief discussion about the effect of tetragonal distortion on SO within the SE model given by Eqs. (1) and (2). For simplicity, rotation and tilt of oxygen octahedron are neglected. Then tetragonal distortion will not mix the three t_{2g} orbitals as long as only the nearest-neighbor hopping is taken into account. With flattened octahedron distortion ($c/a<1.0$), the energy level of d_{xy} orbital is lowered and the hopping integral along c direction t_c is larger than that along a and b directions t_{ab}. This modification in the hopping integral stabilizes C-SO more strongly so long as G-OO is stable. Moreover, as d_{xy} orbital is commonly occupied at all V sites, the lowering of its energy level is favorable to G-OO. On the other hand, elongating distortion ($c/a>1.0$) has a tendency to destabilize G-OO and therefore C-SO because of the destabilization of d_{xy} orbital, Appendix B.

B. Region (c)

Before discussing region (b), we analyze the situation of region (c) in which LVO/LAO is located. With the strong epitaxial strain, the lattice distortion pattern in LVO/LAO is such that the longest V-O bonds at all sites are aligned in the c direction. This FM lattice distortion is observed in all four SOs and induces FM-OO, where d_{yz} and d_{zx} are occupied and d_{xy} is empty for all four V ions, which is directly reflected by the p-DOS of V d orbitals (not shown). G-SO is the most stable magnetic state in this region because such FM-OO produces AF SE interaction mediated by d_{yz} and d_{zx} orbitals. Similarly, using the nonspin-polarized MLWFs in Tables I and II and Fig. 5, the magnetic coupling parameters $J_{12}=J_{34}=10.7$ meV and $J_{13}=J_{24}=8.5$ meV are obtained from Eqs. (1) and (2) and obviously they are consistent with the G-SO ground state.

C. Region (b)

Region (b) is a transient case from region (a) to region (c) as c/a increases. From the discussions so far, we have already noticed that the relative position of d_{xy} energy level plays quite important roles in the determination of the ground-state OO and SO. For $c/a<1.005$, the energy level of d_{xy} is lower than at least either of d_{yz} or d_{zx} after structural optimization, which is consistent with the G-OO in cubic $LaVO_3$ and t-LVO. As c/a increases beyond 1.005, d_{xy} level becomes higher than d_{yz} and d_{zx} levels destabilizing the G-OO and also C-SO. If c/a increases further, d_{xy} orbitals will not be occupied at any V sites and G-SO will be stabilized as already discussed in the preceding section. In either of the cases for d_{xy} orbitals to be fully occupied [region (a)] or fully empty [region (c)], the magnetic coupling within the ab plane is antiferromagnetic. Therefore, partial occupation

of d_{xy} orbitals may be the only possible way of realizing the FM coupling within the *ab* plane which is the case in *A*-SO in region (b).

As discussed in Appendix A, a simple SE model without tilt and rotation of octahedron can also predict a possible stability of *A*-SO in a certain range of elongated tetragonal structure by occupying d_{xy} orbitals alternatingly among the four V sites from V1 to V4 despite the highest orbital energy of d_{xy} among the three t_{2g} orbitals. In this case, the energy cost by the occupation of a higher energy level is compensated by the energy gain in the SE coupling. In this sense, the crystal-field effect and SE coupling are competing. This scenario implies that the appearance of *A*-SO in the phase diagram of Fig. 1 may be a natural consequence of certain degree of tetragonal strain in the strongly correlated d^2 system. However, in this simple model, the stability of *A*-SO is limited in a much narrower range of c/a compared with the result shown in Fig. 1.

In the real system of $LaVO_3$ epitaxially constrained on $SrTiO_3$, coexistence of tilt and rotation of octahedron can produce mixing of d_{xy} with d_{yz} and d_{zx}. However, the effect of such mixing is rather weak as can be seen in Table I and is not sufficient for stabilizing *A*-SO. Using the information about CFOs within nonspin-polarized GGA calculation presented in Fig. 5 and Tables I and II, we estimated the exchange coupling parameters J_{ij} from Eqs. (1) and (2): J_{12} (J_{34}) being 5.7 (6.2) meV and $J_{13}=J_{24}$ being 12.1 meV, respectively. These values correspond to *G*-SO instead of *A*-SO.

The spin-polarized GGA+U calculations show that the d_{xy} occupation depends strongly on SO as clearly seen in the charge density and p-DOS of V ions in Fig. 6. (For FM and *A*-AF, V1 and V4 are in the same category with regard to electron distribution while V2 and V3 are in another category. Therefore, p-DOSs of FM and *A*-AF are shown only for V1 and V2. Similarly only V1 and V3 are shown for *C*-AF and *G*-AF.) As a result, the pattern of oxygen octahedron distortion also depends on SO. It is obvious that under FM SO, d_{xy} orbital is alternatingly occupied on V1 and V2 sites within the *ab* plane, which brings FM in-plane coupling and is consistent with the model analysis mentioned above. On the other hand, in *A*-SO which has the lowest total energy, all the three t_{2g} orbitals are strongly mixed and nearly equally occupied. [Still appreciable variation in the population distribution among four V sites makes OO the *G* type as seen in Fig. 6(b).] Therefore, in order to understand the basic nature of magnetic coupling in region (b), we construct a new set of spin-dependent CFOs which are obtained from MLWFs for spin-polarized t_{2g} bands in GGA+U calculations for each SO of LVO/STO. The on-site energy relative to the Fermi energy and the linear combination coefficients of MLWFs for both spin channels are listed in Table III. One can find that both the on-site energy and the components of each CFO are consistent with the p-DOS shown in Fig. 6. In the energy diagram corresponding to Fig. 3, the t_{2g} atomic orbitals are now replaced with CFOs. The hopping parameters among these CFOs on neighboring sites are also listed in Table IV. Therefore, it is straightforward to calculate the energy gain $-\frac{t^2}{\Delta}$ (t being the hopping parameter between two orbitals separated by energy Δ) in each SO due to virtual

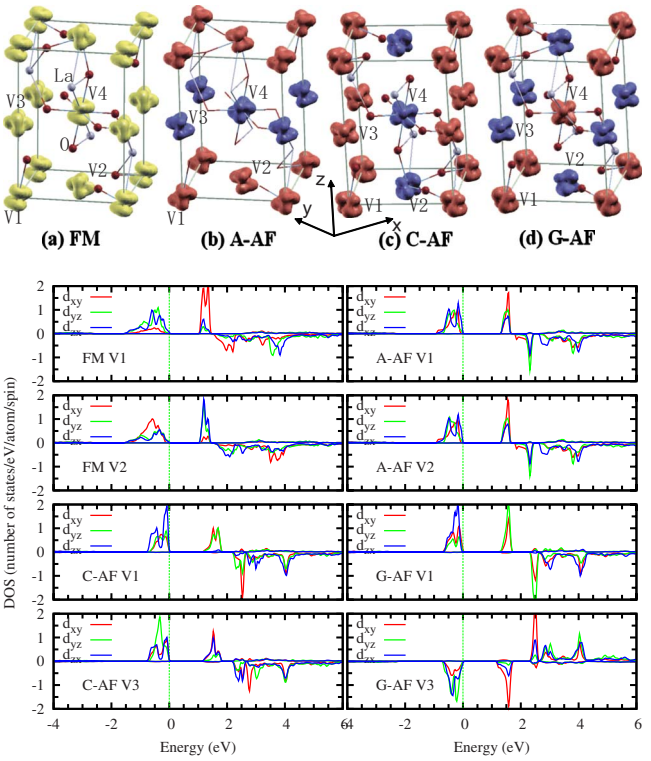

FIG. 6. (Color online) (Upper) The charge density of occupied t_{2g} orbitals in (a) FM, (b) *A*-, (c) *C*-, and (d) *G*-AF LVO/STO. Isovalue for plotting is ± 0.05 e/a.u.^{3} (Lower) The partial density of states of t_{2g} orbitals for selected V ions in FM, *A*-, *C*-, and *G*-AF LVO/STO. Four V sites are labeled as V1, V2, V3, and V4, respectively. The local axes x, y, and z at V sites are defined as the [110], [1$\bar{1}$0], and [001] directions of the unit cell.

hopping paths indicated in Fig. 4. It is found *A*-SO configuration has the largest energy gain, −131.5 meV, among all the four SOs. The smallest one is −91.6 meV in FM case. *C*-SO and *G*-SO have nearly the same energy gain, −113.0 meV and −115.2 meV, respectively. This well explains the total-energy order for LVO/STO in Fig. 1. We have also done similar calculations for t-LVO [region (a)], LVO/LAO [region (c)] as well as $c/a=1.04$ [region (b)]. The ground state of each case does have the largest energy gain and the energy order of the four SOs can also be properly reproduced.

For better understanding of the largest energy gain in *A*-SO, the contribution from each pair to the above energy gain is listed in Table V for LVO/STO. It is interesting to see that the different scheme of d_{xy} occupation between FM-SO and *A*-SO produces comparable energy gain for the FM coupling within the *ab* plane. The main difference in the total-energy gain between them comes from the coupling in the *c* direction. The energy gains by the AF coupling in the *ab* plane for *C*-SO and *G*-SO are also comparable with that of the FM coupling in *A*-SO. Again the stability of *A*-SO with respect to *C*-SO and *G*-SO is due to the coupling in the *c* direction.

As c/a increases, the orbital occupation becomes less sensitive to SO and the details in the contribution from each pair to the total magnetic interaction energy are slightly modified.

TABLE III. The crystal-field orbitals on V ions in MLWF basis for LVO/STO ($c/a=1.01$) in each spin ordering within GGA+U calculations. The on-site energy (in meV) is relative to the Fermi level in each case. Similar as in Fig. 6, only two V sites are shown for each SO.

			Spin up				Spin down			
SO	Site	CFO	On-site energy	d_{xy}	d_{zx}	d_{yz}	On-site energy	d_{xy}	d_{zx}	d_{yz}
FM	V1	CF1	−1149.5	0.025	−0.607	0.795	1702.5	−0.992	−0.120	−0.041
		CF2	−1118.1	−0.291	0.756	0.586	2519.2	0.008	−0.387	0.922
		CF3	597.3	0.956	0.246	0.158	2597.1	−0.126	0.914	0.385
	V2	CF1	−1138.0	0.748	−0.575	0.330	1719.5	−0.370	0.046	0.928
		CF2	−1120.0	−0.587	−0.806	−0.076	2458.8	−0.737	0.593	−0.323
		CF3	593.9	−0.310	0.137	0.941	2578.9	0.565	0.804	0.186
A	V1	CF1	−988.8	0.381	−0.512	0.770	1805.0	0.702	0.709	0.066
		CF2	−964.2	−0.688	0.399	0.606	2598.6	0.428	−0.495	0.756
		CF3	745.9	0.618	0.761	0.200	2701.6	0.569	−0.503	−0.651
	V2	CF1	−989.1	0.371	−0.768	0.522	1803.5	0.725	−0.077	−0.685
		CF2	−963.7	−0.680	−0.607	−0.411	2599.2	0.376	−0.789	0.486
		CF3	744.8	−0.633	0.202	0.747	2700.5	−0.578	−0.610	−0.543

Nevertheless, it is important to note that the partial occupation of d_{xy} orbital is crucial to the stability of *A*-SO state. The mixing of three t_{2g} orbitals is not only related to the lattice distortion but also controlled by strong Coulomb interaction. If the crystal-field splitting and the SE magnetic coupling are comparable in magnitude and they produce competing effects, the lattice distortion and SO should be treated on the equal footing.

IV. CONCLUSION

Based on the GGA+U calculations, we have studied the evolution of SO and OO of $LaVO_3$ as a function of tetragonal strain in the range of 0.98 (bulk $LaVO_3$ case) $\leq c/a < 1.107$ ($LaVO_3/LaAlO_3$ case). For $0.98 \leq c/a < 1.005$, $LaVO_3$ has *G*-OO and *C*-SO. In this case, *G*-OO induces *G*-type JT distortion, which stabilizes *C*-SO further. In this sense, crystal field works *collaboratively* with SE interaction to enhance the stability of *G*-OO and *C*-SO. For $1.005 < c/a < 1.095$, *A*-SO is the lowest energy configuration. $LaVO_3$ grown on $SrTiO_3$ corresponds to $c/a=1.01$. In this range, the d_{xy} level becomes higher than those of d_{yz} and d_{zx}. An analysis based on a simple SE model also predicts stability of *A*-SO when c/a is slightly larger than 1.0. In this analysis, d_{xy} orbital is alternatingly occupied among four V sites. The energy cost of occupying higher level of d_{xy} is compensated by SE interaction. In this sense, crystal-field effect and SE interaction competes. In the GGA+U calculations with full structural optimization, the occupied orbitals and unoccupied one are characterized by strong mixture of three t_{2g} orbitals and the OO is fairly sensitive to SO. An analysis based on the MLWFs constructed from spin-

TABLE IV. The hopping integrals (in meV) between spin-polarized crystal-field orbitals for LVO/STO ($c/a=1.01$).

			V1-V2			V4-V3			V1-V3			V2-V4		
SO	Spin		CF1	CF2	CF3	CF1	CF2	CF3	CF1	CF2	CF3	CF1	CF2	CF3
FM	Up	CF1	−98.3	−39.7	83.6	−71.2	−46.5	96.7	−122.0	−156.9	34.1	−131.8	49.4	−44.4
		CF2	91.2	25.8	−124.0	9.5	−33.9	127.2	52.6	−82.7	−133.9	−149.0	−85.5	24.6
		CF3	−77.8	159.0	22.9	181.9	−50.7	−9.5	45.5	−22.1	−14.7	−31.4	133.0	−13.9
	Down	CF1	−38.4	−45.4	152.5	−8.0	169.9	−80.3	7.4	29.3	−46.3	−7.2	28.0	−112.0
		CF2	77.6	102.4	−2.1	88.6	−53.7	−34.0	−30.2	154.7	98.0	−29.1	−156.4	51.5
		CF3	−131.8	−66.5	−26.7	118.1	−6.0	18.2	113.4	−50.8	86.7	46.5	−95.8	−88.4
A	Up	CF1	−89.6	−14.9	144.7	2.7	−144.8	−122.0	42.2	173.9	−37.1	−41.3	−173.2	40.5
		CF2	26.2	−37.9	−109.1	15.4	84.1	11.1	−92.8	26.5	−115.7	94.5	−24.2	115.6
		CF3	9.3	158.1	16.9	−143.0	7.5	6.2	−23.5	−42.6	−87.6	−23.4	−42.5	−86.0
	Down	CF1	−26.3	23.1	145.9	−98.0	14.4	−47.6	65.6	−67.8	−22.3	67.2	64.1	22.3
		CF2	−147.3	−78.2	−4.6	25.5	48.0	−149.2	−154.7	−86.6	43.0	−150.5	98.3	−39.5
		CF3	−123.0	−5.1	−7.5	172.7	−50.5	−1.0	−7.6	121.3	92.0	18.1	117.4	95.0

TABLE V. The energy gain (in meV) from each virtual hopping between spin-polarized crystal-field orbitals in LVO/STO ($c/a=1.01$) in different SOs.

		FM-SO	*A*-SO	*C*-SO	*G*-SO
LVO/STO $c/a=1.01$		Spin up/down	Spin up/down	Spin up/down	Spin up/down
ab plane	V1-V2	−31.2/0.0	−33.7/0.0	−20.0/−15.2	−18.4/−14.8
	V3-V4	−35.4/0.0	0.0/−33.0	−15.5/−15.5	−15.3/−15.1
c direc.	V1-V3	−12.6/0.0	−16.4/−16.0	−24.7/0.0	−13.3/−12.2
	V2-V4	−12.4/0.0	−16.3/−16.0	−22.3/0.0	−11.7/−14.2
Total-energy gain		−91.6	−131.5	−113.0	−115.2

polarized GGA+U calculations can successfully explain the stability of *A*-SO. It is important to note that in both approaches, d_{xy} orbitals are partially occupied and that this aspect is crucial to the stability of *A*-SO. For $c/a>1.095$, crystal-field effect overwhelms the SE interaction and *G*-SO becomes the ground state. $LaVO_3$ grown on $LaAlO_3$ is in this range.

These results are at least qualitatively consistent with the experimental observation that the interface with $SrTiO_3$ can be metallic while that with $LaAlO_3$ is insulating because the FM intraplane SO within the interface VO_2 layer will become metallic more easily than the AF intraplane SO. Moreover, the observation of anomalous Hall effect for the interface with the $SrTiO_3$ substrate implies that the FM SO must exist at the interface. This is compatible with *A*-SO but incompatible with *C*-SO and *G*-SO.

ACKNOWLEDGMENTS

The authors thank S. Ishibashi for the use of QMAS code and T. Ozaki for the use of OPENMX code in the present work. Their valuable discussions and comments are also appreciated. H.W. acknowledges the Research Promoting Expense from JAIST. The numerical calculations were performed using supercomputers at the Center for Information Science in JAIST and the Information Initiative Center in Hokkaido University. This work is partly supported by the Next Generation Supercomputing Project, Nanoscience Program from the Ministry of Education, Culture, Sports, Science and Technology, Japan.

APPENDIX A: MODEL ANALYSIS OF MAGNETIC PHASES OF $LaVO_3$ WITH TETRAGONAL STRAIN

In this appendix, we try to analyze the general trend seen in Fig. 1 using a simple SE model in which only the tetragonal strain of the lattice is taken into account and tilt and rotation of octahedron are absent. In the evaluation of crystal-field splitting and hopping integrals, we perform nonspin-polarized GGA calculations for artificial $LaVO_3$ with only tetragonal strain for a given c/a and obtain the corresponding CFOs through the construction of MLWFs. Then using Eqs. (1) and (2) supplemented by the crystal-field splitting, we search all the possible combinations of OO and SO for the four V ions.

In the cubic symmetry case ($c/a=1.0$), as already pointed out in the text, the combination of *G*-OO and *C*-SO is the most stable for $0<J_H/U<0.24$. The actual $LaVO_3$ is in this range. For $0.24<J_H/U<0.33$, FM-SO is the most stable. This result suggests that even cubic $LaVO_3$ without JT distortion will take the *G*-OO and *C*-SO as the ground state.

In a weak tetragonal case with $1.0<c/a<1.04$, the *A*-SO becomes the most stable phase if J_H/U is in a proper region (this depends on the c/a value, e.g., when $c/a=1.01$ (corresponding to LVO/STO), $0.16<J_H/U<0.24$). The *A*-SO is accompanied by alternating occupation of d_{xy} orbital on neighboring sites in the *ab* plane. The energy cost of occupying higher d_{xy} orbital is compensated by energy gain from SE interaction involving virtual hopping between occupied d_{xy} orbital on one site and the empty one on the neighboring site.

If $c/a>1.04$, *G*-SO becomes the most stable phase for $J_H/U<0.24$ and the corresponding orbital ordering is FM type with d_{zx} and d_{yz} occupied on all four V sites. Occupation of higher d_{xy} orbital is unfavorable because the crystal field overwhelms the SE interaction and suppresses the orbital fluctuation.

These results presented above are qualitatively consistent with the phase diagram in Fig. 1. Therefore, the sequence of *C*-SO, *A*-SO, and *G*-SO with increase in c/a may be a natural trend. However, in this model analysis, the intermediate region (b) is too narrow compared with that obtained by the GGA+U calculations with full structural optimization. As pointed out in the text, partial occupation of d_{xy} orbital is crucial to the stability of *A*-SO. The tilt and rotation of octahedron enhance the mixture of three t_{2g} orbitals, not only through the direct mixture of orbitals due to lower symmetry but also through the local relaxation of the tetragonal constraint on each octahedron.

APPENDIX B: TETRAGONAL DISTORTION AND $GdFeO_3$ DISTORTION

The model analysis in Appendix A with only tetragonal distortion taken into account gives a very narrow range of c/a ($1.00<c/a<1.04$) in which *A*-SO can be ground state. In the phase diagram of Fig. 1, region (b) is quite broad. In addition to the effect of strong correlation effect, it is also interesting to see how other type of lattice distortion affects the CFOs. In all the cases studied the oxygen octahedra ro-

tate and tilt in the $GdFeO_3$ type. As c/a increases from 0.98 to 1.11, the rotation angle increases from 9.1° to 11.4° while tilting decreases from 13.1° to 9.5°. The distances from V to its eight neighboring La change by ~0.04 Å, about 1%. One can expect that the main changes in the electronic structures mostly come from the local octahedron distortion, which varies from being flattened by about 4% (measured by the difference between the longest V-O bond length and the shortest one) in t-LVO to being elongated by 1% in LVO/STO and 9% in LVO/LAO. In Refs. 18 and 22, the role of $GdFeO_3$-type distortion in the observed SO and OO in RVO_3 (R being rare-earth elements or Y) was discussed. To separate the effect of octahedron rotation and tilting, and local tetragonal octahedron distortion, we have studied several $LaVO_3$ with hypothetical structure which have either tetragonal octahedron distortion or octahedron rotation or tilting. We take the average V-O bond length of LVO/STO, 2.005 Å, and construct the cubic $LaVO_3$, rotated $LaVO_3$ by about 12° ($a^0a^0c^+$) and tilted $LaVO_3$ by 12° ($a^-a^-c^0$).[38] All of them have undistorted octahedra. The angle 12° is taken from experimental $LaVO_3$ structure.[22] Another two $LaVO_3$ experience the compressive (c/a=1.09) and tensile (c/a =0.96) strain to the extent similar to LVO/LAO and t-LVO, respectively, with neither rotation nor tilting. The obtained

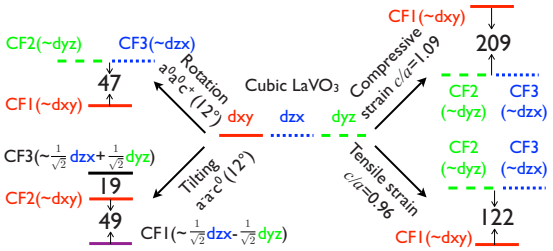

FIG. 7. (Color online) The CF orbitals and splittings (in meV) of $LaVO_3$ with octahedral rotation and tilting by 12° and that under compressive and tensile strain.

CF splittings and orbitals are shown in Fig. 7. Except in the tilting case, the CF orbitals are the same as the MLWFs. In the tilting case, the d_{yz} and d_{zx} orbitals form new CF orbitals lying in two perpendicular La-V planes, formed by the La^{3+} ions which have short and long La-V distances, respectively. Rotation and tilting of octahedra have different effects on d_{xy} orbital. Obviously, in real system when all these distortions coexist, the CF orbitals and splittings closely depend on the details of the geometrical structure.

*Corresponding author; hmweng@jaist.ac.jp

[1] A. Ohtomo and H. Y. Hwang, Nature (London) **427**, 423 (2004).
[2] N. Nakagawa, H. Y. Hwang, and D. A. Muller, Nature Mater. **5**, 204 (2006).
[3] S. Thiel, G. Hammerl, A. Schmehl, C. W. Schneider, and J. Mannhart, Science **313**, 1942 (2006).
[4] M. Basletic, J.-L. Maurice, C. Carretero, G. Herranz, O. Copie, M. Bibes, E. Jacquet, K. Bouzenhouane, S. Fusil and A. Barthelemy, Nature Mater. **7**, 621 (2008).
[5] O. Copie, V. Garcia, C. Bodefeld, C. Carretero, M. Bibes, G. Herranz, E. Jacquet, J.-L. Maurice, B. Vinter, S. Fusil, K. Bouzehouane, H. Jaffres, and A. Barthelemy, Phys. Rev. Lett. **102**, 216804 (2009).
[6] Y. Hotta, Y. Mukunoki, T. Susaki, H. Y. Hwang, L. Fitting, and D. A. Muller, Appl. Phys. Lett. **89**, 031918 (2006); Y. Hotta, T. Susaki, and H. Y. Hwang, Phys. Rev. Lett. **99**, 236805 (2007).
[7] A. Kalabukhov, R. Gunnarsson, J. Börjesson, E. Olsson, T. Claeson, and D. Winkler, Phys. Rev. B **75**, 121404(R) (2007); W. Siemons, G. Koster, H. Yamamoto, W. A. Harrison, G. Lucovsky, T. H. Geballe, D. H. A. Blank, and M. R. Beasley, Phys. Rev. Lett. **98**, 196802 (2007).
[8] G. Jackeli and G. Khaliullin, Phys. Rev. Lett. **101**, 216804 (2008).
[9] U. Lüders, W. C. Sheets, A. David, W. Prellier, and R. Frésard, Phys. Rev. B **80**, 241102(R) (2009).
[10] Q. Gan, R. A. Rao, C. B. Eom, J. L. Garrett, and M. Lee, Appl. Phys. Lett. **72**, 978 (1998).
[11] Z. Fang, I. V. Solovyev, and K. Terakura, Phys. Rev. Lett. **84**, 3169 (2000); B. R. K. Nanda and S. Satpathy, Phys. Rev. B **78**, 054427 (2008).
[12] P.-H. Xiang, H. Yamada, A. Sawa, and H. Akoh, Appl. Phys. Lett. **94**, 062109 (2009).
[13] H. Tsukahara, S. Ishibashi, and K. Terakura, Phys. Rev. B **81**, 214108 (2010)..
[14] H. Sawada, N. Hamada, K. Terakura, and T. Asada, Phys. Rev. B **53**, 12742 (1996); H. Sawada and K. Terakura, *ibid.* **58**, 6831 (1998).
[15] Z. Fang and N. Nagaosa, Phys. Rev. Lett. **93**, 176404 (2004).
[16] G. Khaliullin, P. Horsch, and A. M. Oleś, Phys. Rev. Lett. **86**, 3879 (2001); G. Khaliullin, Prog. Theor. Phys. Suppl. **160**, 155 (2005).
[17] C. Ulrich, G. Khaliullin, J. Sirker, M. Reehuis, M. Ohl, S. Miyasaka, Y. Tokura, and B. Keimer, Phys. Rev. Lett. **91**, 257202 (2003); P. Horsch, G. Khaliullin, and A. M. Oleś, *ibid.* **91**, 257203 (2003).
[18] P. Horsch, A. M. Oleś, L. F. Feiner, and G. Khaliullin, Phys. Rev. Lett. **100**, 167205 (2008).
[19] K. I. Kugel' and D. I. Khomskii, Sov. Phys. Usp. **25**, 231 (1982); Sov. Phys. Solid State **17**, 285 (1975).
[20] Y. Tokura and N. Nagaosa, Science **288**, 462 (2000).
[21] L. D. Tung, A. Ivanov, J. Schefer, M. R. Lees, G. Balakrishnan, and D. McK. Paul, Phys. Rev. B **78**, 054416 (2008).
[22] M. De Raychaudhury, E. Pavarini, and O. K. Andersen, Phys. Rev. Lett. **99**, 126402 (2007).
[23] T. Higuchi, Y. Hotta, T. Susaki, A. Fujimori, and H. Y. Hwang, Phys. Rev. B **79**, 075415 (2009); E. Dagotto, Phys. **2**, 12 (2009).
[24] The volume conservation corresponds to the Poisson ratio γ of 0.5. Unfortunately we have no information about the actual value of γ for $LaVO_3$. Even if γ may deviate from 0.5 slightly, the results of the present calculations are qualitatively correct. However, the critical value of c/a corresponding to the phase boundary depends on γ. For example, if γ may be 0.7, which is the value for $La_{1-x}Sr_xMnO_3$ (Ref. 25), the c/a value for $LaVO_3$

grown on $LaAlO_3$ becomes 1.086, which is in the region (b) of Fig. 1. However, the whole total-energy curves are modified slightly by changing γ. We have confirmed that even with $\gamma=0.7$, the ordering of total energies for different SOs remain the same as that in Fig. 1 with $\gamma=0.5$ for $LaVO_3$ grown on $LaAlO_3$ though the energy difference between *G*-SO and *A*-SO is reduced to only 3 meV/f.u.

[25] Y. Konishi, Z. Fang, M. Izumi, T. Manako, M. Kasai, H. Kuwahara, M. Kawasaki, K. Terakura, and Y. Tokura, J. Phys. Soc. Jpn. **68**, 3790 (1999).

[26] http://qmas.jp/

[27] J. P. Perdew, K. Burke, and M. Ernzerhof, Phys. Rev. Lett. **77**, 3865 (1996).

[28] S. L. Dudarev, G. A. Botton, S. Y. Savrasov, C. J. Humphreys, and A. P. Sutton, Phys. Rev. B **57**, 1505 (1998).

[29] N. Marzari and D. Vanderbilt, Phys. Rev. B **56**, 12847 (1997); I. Souza, N. Marzari, and D. Vanderbilt, *ibid.* **65**, 035109 (2001).

[30] http://www.openmx-square.org/

[31] H. Weng, T. Ozaki, and K. Terakura, Phys. Rev. B **79**, 235118 (2009).

[32] E. Pavarini, S. Biermann, A. Poteryaev, A. I. Lichtenstein, A. Georges, and O. K. Andersen, Phys. Rev. Lett. **92**, 176403 (2004); E. Pavarini, A. Yamasaki, J. Nuss, and O. K. Andersen, New J. Phys. **7**, 188 (2005); M. Mochizuki and M. Imada, *ibid.* **6**, 154 (2004).

[33] In GGA+*U* calculation by OPENMX, the effective Coulomb parameter *U* is taken to be 2.0 eV rather than 3.0 eV in the corresponding calculation by QMAS. This difference in *U* between the two codes comes from the fact that OPENMX uses atomic orbital-like basis set while QMAS is based the PAW method with the plane-wave basis. Therefore *U* is applied to the atomic-orbital-like basis in OPENMX and to the smaller augmentation region in QMAS. We confirmed that two results by two calculations are very similar.

[34] I. V. Solovyev, Phys. Rev. B **74**, 054412 (2006).

[35] T. Mizokawa and A. Fujimori, Phys. Rev. B **54**, 5368 (1996).

[36] In Eqs. (1) and (2), contributions from pair excitations to intermediate states are included while they are not taken account of in the exchange passes shown in Fig. 4.

[37] The hopping integrals between obtained MLWFs decay quickly as the distance between MLWFs increases. For example, in the case of t-LVO, hopping integral between nearest-neighboring (NN) d_{zx} is -0.214 eV. Those of next-nearest-neighbor (NNN), and the third-nearest neighbor (3rd-NN) are 0.004 eV and 0.0001 eV, respectively. That of d_{xy} for NN, NNN, and 3rd-NN is 0.155 eV, -0.047 eV, and -0.012 eV, respectively. The NN approximation is justified since the largest omitted contribution to spin-orbital superexchange interaction is $2.0(-0.047)^2/3.0 \approx 1.5$ meV.

[38] As for the notation such as $(a^0a^0c^+)$, see P. W. Woodward, Acta Crystallogr., Sect. B: Struct. Sci. **53**, 32 (1997).